Thirteenth International Symposium on Space Terahertz Technology, Harvard University, March 2002.

Improved Equivalent Circuit for Hot Electron Bolometer Mixers Fed by Twin Slots

Paolo Focardi, Andrea Neto, William R. McGrath, Bruce Bumble, Henry G. LeDuc

Abstract— **Series-fed coplanar waveguide embedding circuits are recently being developed for terahertz mixers using, in particular, superconducting devices as sensors. Although these mixers show promising performance, they usually also show a considerable downward shift in the resonating frequency, when compared with calculations using simplified models. This effect is basically caused by parasitics due to the extremely small details (in terms of wavelength) of the device and by the impedance of the remaining embedding circuit (in particular the RF filter). In this paper, we present an improved equivalent network model of such devices which agrees with measured results. We first propose a method to calculate the characteristic impedance and the propagation constant of the coplanar waveguide, etched between two semi-infinite media, that connect the receiving slot antennas to the superconducting device. In the formulation we take into account, for the first time, the radiation power leakage. We then describe the procedure to calculate the reactances due to the detailed geometry of the mixer device and circuit and we correct the input impedance, calculated with a commonly used simplified network. By comparing our results with a complete set of measured data, for seven mixers in the range between 500 GHz and 3 THz, we analyze the features of our model and propose further improvements. Indeed, based on the good results obtained with our improved equivalent network, a new set of THz mixers has been fabricated and is currently being tested. Useful guidelines for designing THz mixer circuits are also given.**

I. Introduction

SLOT antennas coupled to coplanar waveguides (CPW) are being developed for quasi-optical single-pixel heterodyne detectors for use in atmospheric and astronomical instruments in the submillimeter-wave/terahertz-frequency range. Hot Electron Bolometer (HEB) mixers ([1], [2]), for example, are often used at THz frequencies in such circuits placed at the focus of a dielectric lens ([3], [4]). HEB receivers are already finding use up to 1 THz on ground-based radiotelescopes [5], and similar receivers are being developed for frequencies up to 2 THz for the ESA/NASA Herschel Space Observatory, and up to 3 THz for NASA's SOFIA aircraft observatory.

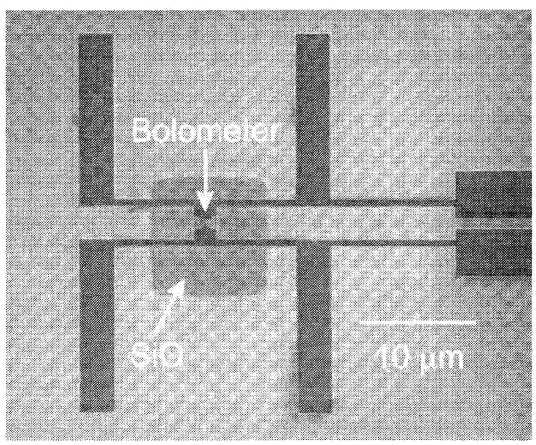

Fig. 1. Scanning Electron Microscope (SEM) photograph of an HEB mixer embedding circuit. The superconducting device is located at the center and coupled to the twin-slot antenna via CPW lines.

The prediction of the radiation pattern (up to 500 GHz) and of the resonating frequency (up to 100 GHz) for these mixer circuits has been found to be accurate, with respect to measurements, using a simplified network [6]. However, when the device is operated well into the THz regime (up to 2.5 THz), the measured resonant frequency (i.e. frequency of the peak response of the detector) is often significantly lower than that calculated with simple models ([2], [7]). This leads to significant increases (up to a factor 2) in

P. Focardi, W. R. McGrath, B. Bumble and H.G. LeDuc are with the Jet Propulsion Laboratory, California Institute of Technology, 4800 Oak Grove Dr., Pasadena, 91109 CA.

A. Neto is with FEL-TNO, Den Haag, The Netherlands.

mixer noise due to the reduction in coupled signal power at the desired THz frequency. Thus, as previously reported [7], the accurate characterization of the entire mixer embedding circuit, including the parasitics associated with the geometry of the device, is needed to correctly design the circuit. Even though the geometry of these antennas, CPW lines, and devices is relatively simple, accurately simulating their performance in a THz circuit is not a straightforward matter. To the knowledge of the authors there are no commercial software tools to tackle this problem, even more so when the lens effect also has to be included [6]. A brute force approach based on a Method of Moments (MoM) analysis of the overall planar structure can be used, but since the device dimensions can be of the order of $\lambda_0/1000$, the numerical effort required for an accurate analysis becomes almost prohibitive, even for a single antenna. In [8] a dedicated MoM scheme for this kind of structure has been presented.

In this paper an equivalent network is presented that significantly improves the one presented in [6], though the lens effect is not included in order to concentrate the attention to the feed mechanism. The model is improved in the sense that the radiation leakage is accounted for in the calculation of the transmission line parameters. Additionally, the transition between the CPW and the bolometer is characterized via analytically evaluated lumped reactances. The emphasis is given to the physical interpretation rather than to the numerical solution (as in [8]), since this is what will be useful in future designs. A complete and detailed formulation of the improved equivalent network parameters has been presented in a recent publication [9]. In this paper we describe the procedure for calculating the above parameters, without getting into the mathematical details. In section II we first briefly describe the geometry of the detectors and circuits. Then, in section III, the formulation to calculate the parameters of the equivalent network is described. Before this work, the quasi-static approximations for these parameters were too inaccurate to correctly predict the actual performance of the circuits under investigation. The work in [10] accounts for a complex propagation constant in coplanar lines. However in [10] the attenuation was associated to losses in the conductor and in the dielectric rather than to the radiation effect which appears to be dominant in the case investigated in this paper.

A recent investigation [11] presents a direct integration method for the Green's Function (GF) of a microstrip. In [12] the method has been applied to slots etched between two semi-infinite dielectrics and provides, analytically in that case, the GF of a gap-excited slot placed between two different homogeneous dielectrics. In [9] the procedure is extended to coplanar waveguides in order to derive the circuit parameters mentioned above. Then we present a procedure that characterizes the strong reactive contributions associated with the transition between the bolometer and the coplanar waveguide. The lumped reactances we obtain are connected to the equivalent network that represents the overall antenna+detector circuit. This circuit is composed of the CPW equivalent transmission lines and of the active impedance of the slots; that is, the impedance of each of the two slots with the mutual coupling taken into account. In section IV, comparisons with measurements of submillimeter wave bolometric receivers show that the observed downward shift of the resonant frequency can be explained by the following: I) the reactances associated with both the "crowding" of the RF current and the fringing fields in the transition between the bolometer and the CPW (see fig. 2), and II) the phase shift caused by the imaginary part of the impedance of the RF bandstop filter used in the DC/IF line. In section V, some guidelines for future designs are provided and a new set of THz HEB mixers, that has been fabricated and is currently being tested, is presented. Finally, in section VI conclusions are drawn.

II. Receiver layout

The mixer circuit is located at the second focus on the back side of a silicon elliptical lens. Since the reflections due to the dielectric lens can be introduced separately, as discussed in [6], we assume the circuit under investigation to be located at the interface between two semi-infinite half spaces ($\epsilon_{r1} = 1$ and $\epsilon_{r2} = 11.7$). The spectral response and hence the center frequency of HEB mixers with six different twin-slot antenna designs have been previously measured with a Fourier-Transform Spectrometer [7]. The antenna slot lengths ranged from 26 μm up to 152 μm. Figure 1 shows a SEM photograph of a 2.5 THz HEB mixer.

The submicron-sized HEB device is connected to the twin slot-antennas via a CPW transmission line [1]. On the right, is located the RF band-stop filter structure (a total of eight high and low impedance sections were used). Figure 2 shows a detail of the transition between the CPW and the bolometer. The length of the transition region L and the width of the bolometer w_b are highlighted in the figure. The modeling of this structure could be performed with a full wave Method of Moment analysis as described in [8]. However in this paper we present an equivalent network model for the overall mixer embedding circuit. The first simplified equivalent network is shown in fig. 3.

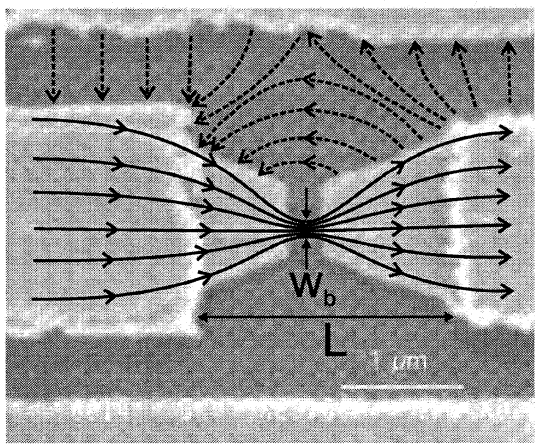

Fig. 2. Bolometer detail of a 2.5 THz design with a schematic representation of the electric field (dashed line) and of the RF current path (solid line).

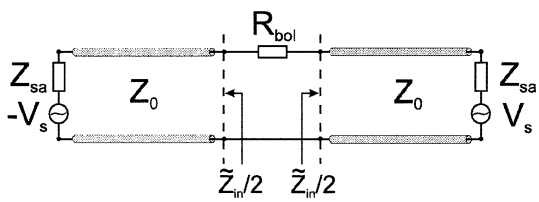

Fig. 3. Simplified equivalent network of the THz mixer circuit which includes the active slot impedance and the equivalent transmission lines.

The active slot impedances Z_{sa} are obtained by means of MoM simulations restricted to the receiving slots alone, while R_{bol}, Z_0 and V_s represent respectively the nominal DC impedance of the bolometer, the characteristic impedance of the CPW and the equivalent voltage source of the receiving antenna.

In the next section the transmission line parameters are presented, taking into account for the first time the power leakage in the two dielectrics. With the simplified equivalent network of fig. 3 we may then estimate the equivalent series load $\tilde{Z}_{in}$ seen by the bolometer. However, $\tilde{Z}_{in}$ must be modified to account for the reactances due the field deformations shown in fig. 2, which are associated with the CPW-to-bolometer transition. Analytical expressions for these reactances are available in [9]. Finally, as discussed in section IV, the effects of the RF filter must also be included to completely characterize $\tilde{Z}_{in}$.

III. Equivalent Network Parameters

The parameters of the CPW transmission line have been obtained using the formalism that has been presented in [12] for the case of a single slot etched in a perfect electric conductor between two semi-infinite dielectrics. In [9] the same formulation is extended to the case of an infinitely extended CPW whose geometry is shown in the inset of fig. 4.

A. Propagation Constant

The quasi-static approximation of the propagation constant is $\beta = \sqrt{\frac{k_1^2+k_2^2}{2}}$ [13], where $k_i = k_0\sqrt{\epsilon_{ri}}$ $(i = 1, 2)$, is the wavenumber in each semi-infinite dielectric (air and silicon) and k_0 is the free space wavenumber. Accordingly, the propagating mode is fast for the denser medium (i.e. silicon) and the mode is leaky. The unknown magnetic currents on the CPW are obtained from the direct solution of the pertinent Continuity of Magnetic Field Integral Equation (CMFIE) assuming, as in [11], the separability between transverse and longitudinal space functional dependence. In particular, the transverse electric field is assumed to be well represented by a unique edge singular function defined on each of the two slots composing the CPW. The procedure for finding the space domain magnetic current consists of: I) expanding via a Fourier Transform the transverse impressed magnetic field in spectral superposition of electric currents progressively phased by k_x; II) finding in analytical form, for each k_x, the 2D Green's Function

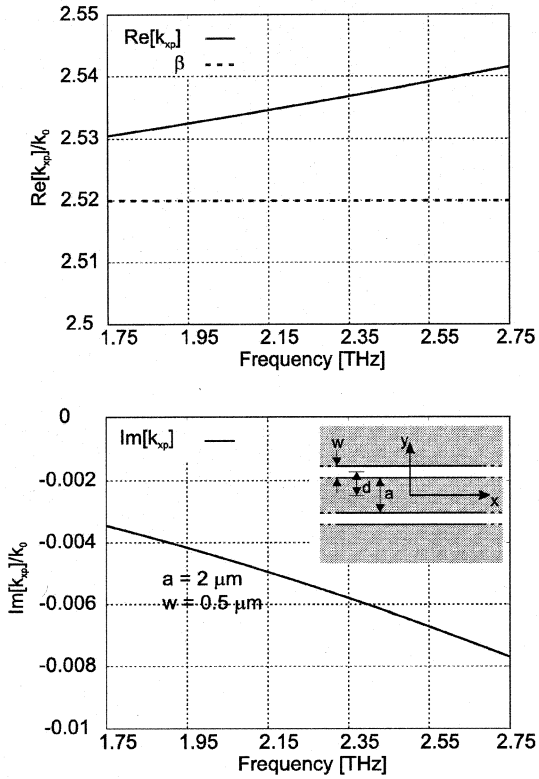

Fig. 4. Real and imaginary part of the propagation constant for a CPW with $a = 2\mu m$ and $w = 0.5\mu m$. Both graphs are normalized to the free space wavenumber. The real part also shows a comparison with the value of β (dashed line), obtained with the quasi static approximation.

(GF) by imposing the continuity of the magnetic field at the slot axis; and III) integrating in k_x all the 2D GF. Equating to zero the denominator of the spectral expression for the magnetic currents, a dispersion equation is obtained that, solved numerically, defines the propagation constant of the leaky mode supported by the structure.

In fig. 4 an example of the propagation constant is shown for a CPW with $a = 2\mu m$ and $w = 0.5\mu m$ (these are typical values for a THz circuit) as sketched in the inset. Both graphs are normalized to the free space wavenumber. In the upper graph, the real part of k_{xp} is shown, compared with the value of β (dashed line), obtained with the quasi static approximation. As the frequency increases the value of $Re[k_{xp}]$ tends asymptotically to the value of the propagation constant in the denser medium (silicon). In the lower graph the attenuation constant ($Im[k_{xp}]$) is seen to change significantly over the frequency range of 1 THz. Despite the amplitude of the real part (in the frequency range under investigation) being only slightly different from the value of the quasi static approximation, the important point is that now we have a frequency dependent function, and even more important is the fact that now we have an imaginary part that takes into account the power leakage.

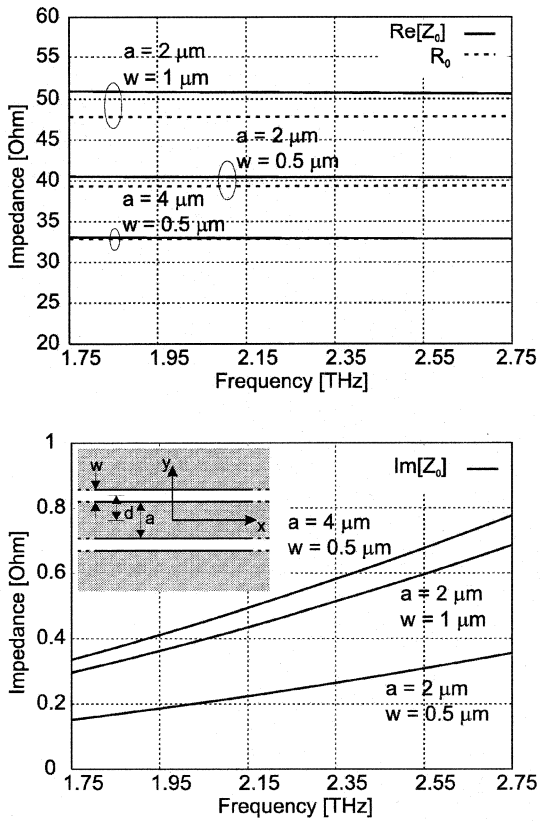

Fig. 5. Real and imaginary part of the CPW characteristic impedance for three different CPW geometries. Also shown in the upper graph, for the real part, is a comparison between the formulation of this paper (solid line) and the quasi static approximation (dashed line).

B. Characteristic Admittance

The definition of the characteristic admittance for a leaky line is a "hot topic" and has been

the subject of recent investigations; particularly promising is the one in reference [14]. In [9] we define the characteristic admittance at a specific transverse section as the ratio between current and voltage of the leaky wave launched by a source at finite distance. This avoids some of the ambiguities that arise with a leaky transmission line when the source is assumed to be at infinite distance. Indeed, since the propagating mode is exponentially attenuated in x, for x tending to infinity the major field contribution on the slot axis are due to fringe currents (that decay as $1/x^2$) rather than to the mode itself [12].

In fig. 5 the characteristic impedance of three different CPW's is shown, along with the values obtained with the quasi-static approximation formulated in [13]. Our formulation provides not only the imaginary part but also it can be seen that the quasi-static formula underestimates the real part of Z_0 when the width of the CPW slots grows with respect to the inner conductor a. In particular, this aspect significantly impacts the simulation results when introducing a transmission line model of the band stop filtering structure.

C. Reactances

The equivalent network in fig. 3 alone provides $\tilde{Z}_{in}$ which does not account for the electric and magnetic current crowding effects occurring in the transition between the bolometer and the CPW. Since the bolometer width is much narrower with respect to the CPW inner conductor, strong reactive energy is concentrated at this transition (see fig. 2). Our analysis accounts for the effect of the transition by correcting $\tilde{Z}_{in}$ via the introduction of two lumped reactances related to the lengths and widths involved in the transition. These two reactances are combined to represent a realistic model of the transition. In this way we can then calculate Z_{in} which is the actual embedding circuit series impedance seen by the bolometer.

With reference to fig. 6, the effect on the input impedance of the electric current crowding associated with an inner conductor reduction ($t_1 \rightarrow t_2$) can be represented as a series inductive impedance Z_s. An infinite slot, whose width is equal to L, is the canonical problem that best fits the geometry in fig. 6. The growth of inductive energy associated with the reduction of the inner conductor

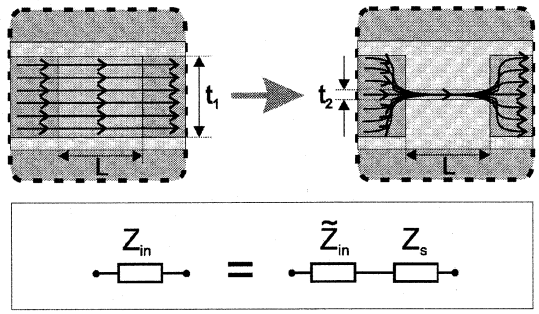

Fig. 6. Electric current crowding effect with the relevant dimensions indicated. In the upper part of the figure the electric current is sketched. In the lower part the connection of Z_s to the equivalent circuit is represented.

from t_1 to t_2 is assumed to be the same as that occurring in the selected canonical problem when the dimension of the source region is reduced accordingly. The complete formulation to derive Z_s is presented in [15] and applied in [9] to the case of a CPW. The series impedance Z_s grows linearly with the length L of the transition and it is also proportional to $ln(t_2)$ as t_2 tends to zero.

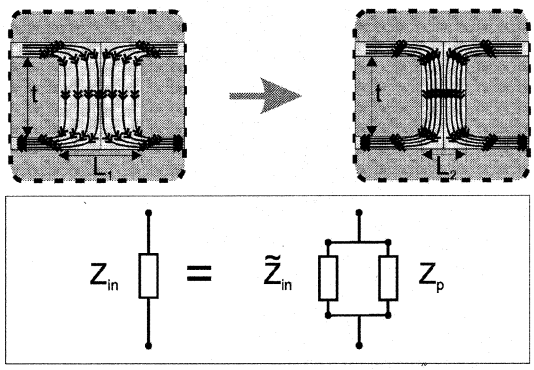

Fig. 7. Magnetic current crowding effect with the relevant dimensions indicated. In the upper part of the figure the magnetic current is sketched. In the lower part the connection of $Z_p = 1/Y_p$ to the equivalent circuit is represented.

With reference to fig. 7, the effect on the input impedance of the magnetic current crowding associated with a gap length shortening ($L_1 \rightarrow L_2$) can be represented as a parallel capacitive admittance Y_p. An infinite dipole printed between two semi-infinite dielectrics, whose width is equal to t, is the canonical problem that best fits the geom-

etry in fig. 7. The growth of capacitive energy in the fringing fields associated with a reduction of the gap from L_1 to L_2 is assumed to be the same as that occurring in this selected canonical problem when the dimension of the source region is reduced accordingly. Y_p is derived in reference [16], and explicitly formulated in [9] for the case of a CPW. The parallel admittance Y_p grows linearly with the width t of the transition. Again, it is proportional to $ln(L_2)$ as L_2 tends to zero.

In order to account for a more general transition we can combine the previous reactances in a staircase form, resulting in an equivalent network as shown in fig. 8. Note that all the parameters of the network are calculated with closed form expressions, provided that the largest dimensions of the transition are approximately less than $\lambda_{eff}/20$, where $\lambda_{eff} = 2\pi/\beta$ and β is the quasi static approximation of the propagation constant.

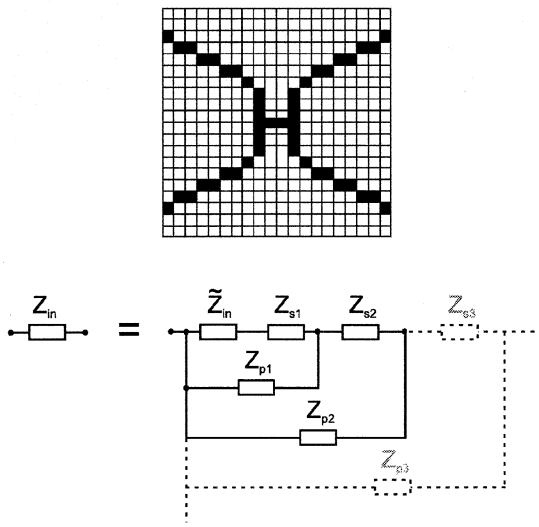

Fig. 8. Example of transition adopted to simulate the actual circuit geometry and of the equivalent network obtained resorting to a "staircase" shaped transition. The layout shown here is representative of the tapered transition region of Mixer No. 1. Each unit represents 0.1 μm.

IV. Numerical results

The parameters of the twin-slot mixers which have been measured and analyzed are shown in fig. 9, along with the bolometer device DC resistance, and in fig. 10 the relevant geometric parameters are indicated. Figure 11 shows the resonance

Mixer	L_a (μm)	W_a (μm)	S_a (μm)	a (μm)	b (μm)	R_{bol} T = 4°K	ν_c Measured (THz)
1	26	3	19	3	4	15	2.22
2	33	3	19	3	4	18	2.19
3	36.5	2	19	2	3	18	2.02
4	36.5	2	19	2	3	25	2.01
5	44	4	25	4.5	6	46	1.60
6	48	2.6	25	3	4.4	25	1.71
7	152	8.3	79.2	8	11	32	0.54

Fig. 9. Parameters of the different mixer circuits under investigation. R_{bol} is the HEB device DC resistance. Refer to fig. 10 for the meaning of the others parameters.

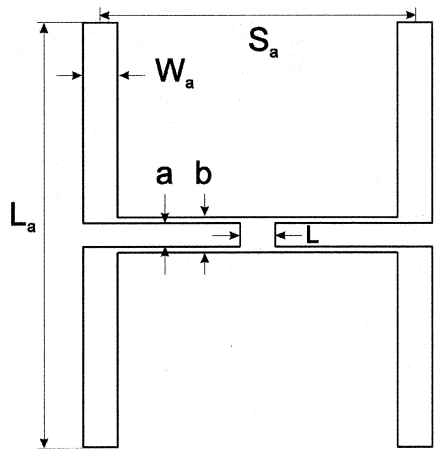

Fig. 10. Schematic layout of physical structure used in the simulations with the relevant dimensions defined.

frequency for the mixers under investigation. The measured results (dashed line with "prism" symbols) are compared with calculated curves that are obtained by using either the simplified network as it is ("plus" symbols) or corrected via the reactive current crowding contributions ("square" symbols). These latter are obtained assuming the flared transition between the bolometer and the inner conductor of the CPW such as in fig. 8, taking into account the actual dimensions of the mixer embedding circuits observed with the Scanning Electron Microscope. While the series inductance of fig. 6 tends to decrease the resonating frequency of the mixer, the parallel capacitance of fig. 7 tends instead to increase it. However, the overall effect, as shown in fig. 11 ("square" sym-

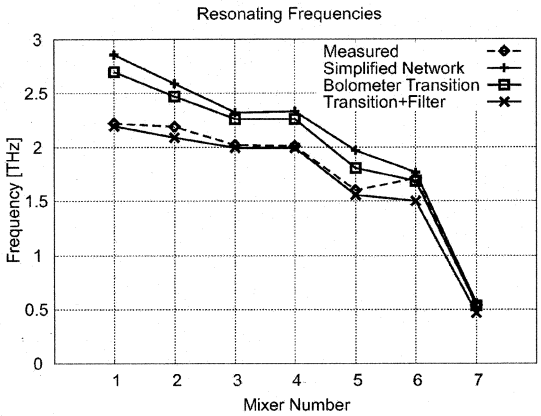

Fig. 11. Summary of measured and calculated resonating frequencies for the seven mixers under analysis.

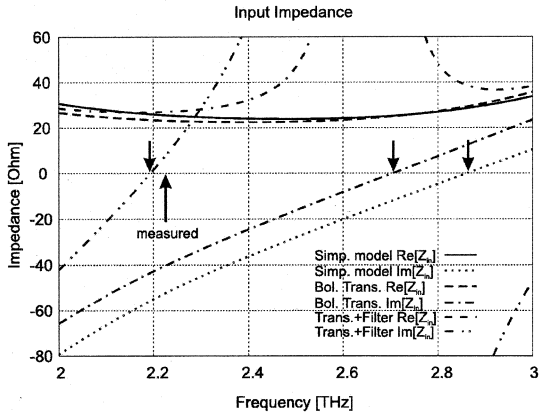

Fig. 12. Input impedance of mixer No. 1 calculated including: 1) simplified network, 2) simplified network + bolometer transition, 3) simplified network + bolometer transition + RF filter.

bols), is that the resonating frequency decreases, with respect to the simplified model. This means that the inductive part of the reactance we introduced tends to prevail.

The resonating frequency is even more strongly affected by the presence of the RF band-stop filter (see Section II). This latter has been modeled by simple transmission line theory where the relevant parameters are evaluated as in Sections III A and III B. Also shown in fig. 11 are the results ("×" symbols) obtained when the impact of the RF filter is included. It is apparent that the agreement between prediction and measurements is outstanding, except for the case of mixer No. 6. These results give strong support to our improved equivalent network, considering the extreme challenges associated with fabrication and measurement at 2.5 THz and the fact that the modeling of the filter does not account for the "step" transitions between the high and low impedance sections. However these latter can be considered higher order effects easily comparable with other phenomena that are not accounted for in the present analysis (i.e. internal reflections inside the lens, gluing of the silicon lens to the chip, fabrication tolerances, variation of metal thickness etc.). It is moreover clear from fig. 13, discussed in the following, that selecting the resonant frequency from the measured peak of the Fourier Transform Spectrometer (FTS) data is not a straightforward matter.

It is useful to refer to the percentage resonating frequency shift as the difference between the predicted and the measured frequency. We may highlight this shift by observing fig. 12 where a detail of the input impedance of mixer No. 1 is shown. Arrows indicate the resonating frequencies, for measured and predicted results, that occur when the imaginary parts of the impedance cross zero. Improving the simplified network with only the effect of the bolometer-CPW transition decreases the shift from 29% to 22%. By further introducing the effect of the filter, the resonant frequency shift decreases to 1%.

In the past the observed shift has been attributed to unknown lumped reactive effects associated to the superconducting bolometer itself (i.e. thermal gradients and skin effects). The present analysis attributes the dominant part of the observed shift to the embedding circuit modeled in this paper. From fig. 12 one can also outline the significant impact of the filter on the real part of the input impedance and the narrowing of the bandwidth due to the several high and low impedance sections used in the filter.

In fig. 13 the FTS direct detection responses of mixer No. 1, 3 and 5 are presented. For the same set of mixers, fig. 14 shows the predicted coupling efficiency, between input and bolometer impedance. These latter are obtained resorting to the following well known impedance-mismatch

expression:

$$\eta = 1 - \left| \frac{R_{bol} - Z_{in}}{R_{bol} + Z_{in}} \right|^2, \qquad (1)$$

where R_{bol} is the resistance of the bolometer and Z_{in} is the series impedance seen by the device in the equivalent circuit. The measured bandwidths appear larger than the calculated ones. This is basically due to the normalization adopted in the FTS curves: these are normalized to the maximum of the peak response while those in fig. 14 reflect the calculated mismatch between bolometer and input impedance. The ripples in the measured curve are due to several effects related to the quasi-optical FTS measurement system, in particular the lens internal reflections [6] and the thickness of the glue layer holding the chip to the lens.

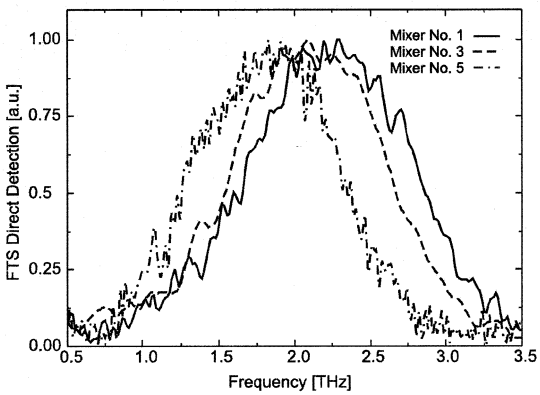

Fig. 13. Measured FTS direct detection responses for mixer No. 1, 3 and 5.

V. Design Considerations

Based on the previous results some guidelines for future design of CPW based twin slot bolometric mixers are now given.

In the past ([4], [6]), the main constraint in the design of such a mixer has been the overall beam pattern of the antennas+lens system, the emphasis being given to a gaussian shaped beam and consequently, good radiation efficiency. This goal was achieved operating the twin slot antenna at its second resonance. In this way a low real part of the input impedance for each slot was obtained

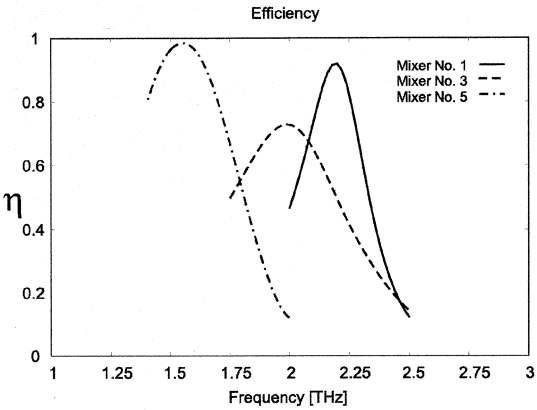

Fig. 14. Calculated coupling efficiency curves for mixers No. 1, 3 and 5.

and a good match to the characteristic impedance of the CPW could be achieved (each one in the order of 40 Ohms). More problematic instead was the matching between the bolometer impedance (typically low to obtain a fast response from the device) and the equivalent load represented by the CPW and slot antennas on each side of the bolometer. Moreover, the non zero reactance, provided by the RF filter, could significantly affect the impedance of the equivalent load of the slot connected to the filter itself. This latter effect and the CPW-bolometer transition play a dominant role in explaining the downward shift of the resonating frequency shown by the mixers under investigation.

As a result of the present investigation it seems more convenient to operate the slot antennas on their first resonance (half instead of a full wavelength long slots). Indeed, even though the overall radiation pattern could be slightly affected and different from the theoretical optimum, the input impedance of the radiating slots turns out to be higher (about 140 Ohms for the real part of mixer No. 1 at 2.5 THz). In this way the slot input impedance is more stable and the impact of the imaginary part of the filtering structure is less significant because it is in series to a high impedance.

To further motivate this choice it is worth mentioning that the previous studies on the beam efficiency [4] were based on Physical Optics (PO) calculations of the radiation patterns. There are presently on-going studies that include more so-

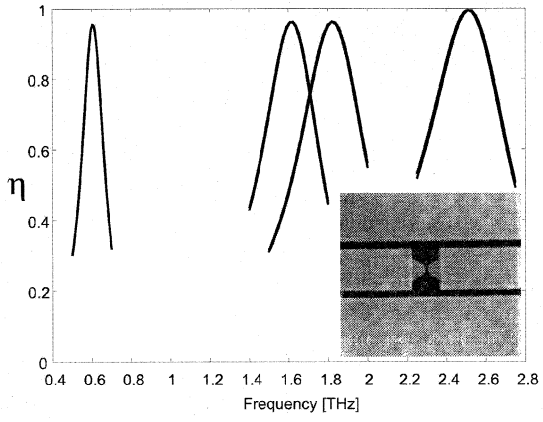

Fig. 15. Calculated matching efficiency between the bolometer resistance and the equivalent input impedance seen by the bolometer itself: new tapered designs.

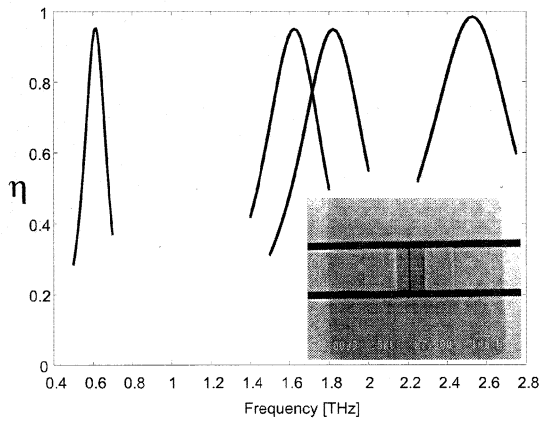

Fig. 16. Calculated matching efficiency between the bolometer resistance and the equivalent input impedance seen by the bolometer itself: new non-tapered designs.

phisticated diffraction mechanisms [17]. These latter could affect the calculation of the optimum beam efficiency for these kind of lenses. Additionally, when the slot antennas are operated on their first resonance, the slot impedance presented to the bolometer via a $\lambda_{eff}/4$ long CPW transmission line is much lower and typically about 20 Ohms. This way a good match of the real part of this impedance with that of the bolometer is straightforward, which results in a nearly optimum efficiency. It is true that in this configuration the impact of the lumped reactances associated with the CPW-bolometer transition are more relevant. However, observing the analytical expressions of the impedances presented in Section III C and explicitly formulated in [9], it is clear that the effect of this transition is much more negligible if the length of the transition L is reduced to the minimal realizable dimension without resorting to the flared transition of fig. 2.

Based on the previous considerations and on the good results obtained, a new set of THz mixers has been fabricated and is currently being tested. Different designs at four center frequencies have been carried out; in particular we aimed to have the center frequency at: 0.6, 1.6, 1.8 and 2.5 THz. The bolometer has been fabricated in Niobium and the microbridge is always 0.1 μm wide, while the length has been chosen to be either 0.1 or 0.2 μm. Moreover, with this new set of mixers we designed two different transitions between the CPW inner conductor and the bolometer: a tapered one, like in the previous measured devices, and a new non-tapered one. The choice of a non-tapered transition has been suggested by the formulation presented in [9] and is expected to give a much more negligible lumped reactance in the equivalent circuit and therefore a smaller down shift in the resonating frequency. Finally, also the filter section has been re-designed accordingly.

In fig.s 15 and 16 the calculated matching efficencies of the new designs are shown. In particular it is worth noting the example of the new non-tapered transition in the inset of fig. 16 and the very accurate and sharp profile of the 0.1 μm gap in the CPW inner conductor obtained with the fabrication process. These results, besides being very promising are also very useful for predicting the expected bandwidth of the receivers, even though other effects (such as the silicon lens effect) are not included in the model presented in this paper.

VI. Conclusions

In this paper we have presented an improved model for series fed coplanar waveguide embedding circuits that are used in bolometric THz receivers. We first calculated the complex propagation constant and characteristic impedance of the weakly leaky mode propagating in the CPW etched between two semi-infinite dielectrics. It has been found that for higher values of the charac-

teristic impedance the quasi static approximation is inadequate for an accurate design that aims to match the CPW impedance to the radiating slots or to the bolometer. We have also presented an improved model of the planar transition between the CPW and the bolometer.

Using these improvements, we have investigated seven mixers developed for real instrument applications and we have been able to explain the downward shift in the resonating frequency when comparing simplified predictions with the actual measurements. Higher order physical effects that can contribute to the input impedance of the circuit are still not taken into account. In particular, the bolometer impedance is accurately known only in DC and it is not necessarily real at 2.5 THz. Skin effects could have an impact on the overall circuit and other reactances could be associated with the vertical variation of the metal thickness between the CPW inner conductor and the superconductive metal of the HEB device. Finally, the transitions between high and low impedance sections of the filter should be taken into account.

Nevertheless the results obtained by our improved equivalent network are outstanding considering the extreme challenges associated with fabrication and measurement at 2.5 THz, and the predictions obtained for the new set of THz mixers presented in the last section of this paper are very promising.

Acknowledgments

This research was performed at Jet Propulsion Laboratory, California Institute of Technology, under contract with the National Aeronautics and Space Administration.

References

[1] B.S. Karasik, M.C. Gaidis, W.R. McGrath, B. Bumble, H.G. LeDuc, *Low noise in a diffusion-cooled hot-electron mixer at 2.5 THz*, Applied Physics Letters, 71, 1567, (1997).

[2] W.F.M. Gonzeules, J.R. Gao, W.M. Laauwen, G. de Lange, T.M. Klapwijlc, P.A.J. del Corte, *Direct and Heterodyne Response of Quasioptical Nb Hot Electron Bolometer Mixers Designed for 2.5 THz Radiation Detection*, Proceedings of the 11th International Symposium on Space Terahertz Technology, Univ. of Michigan, Ann Arbor, pp. 69-81, May 2000.

[3] D.B. Rutledge, D.P. Neikirk and D.P. Kasiligan, *Integrated Circuit Antennas*, in "Infrared and millimeter-waves", K.J. Button, Ed. New York: Academic, 1983, Vol. 10, pp. 1-90.

[4] D.F. Filippovic, S.S. Gearhart and G. M. Rebeiz, *Double-Slot Antennas on Extended Hemispherical and Elliptical Silicon Dielectric Lenses*, IEEE Trans. on Microwave Theory and Techniques, Vol. 41, Oct. 1993, pp. 1738-1749.

[5] J. Kawamura, T. Hunter, C.-Y.E. Tong, R. Blundell, D.C. Papa. F. Patt, W. Peters, T. Wilson, C. Henkel, G. Gol'tsman, E. Gershenzon, *Ground-based Terahertz Spectroscopy Towards Orion*, Accepted for publication in Astronomy and Astrophysics Letters, pp. XXX - XXX (2001).

[6] M. Van der Vorst, P.J.I. De Maagt, A. Neto, A. Reynolds, W. Luinge, R. Heres, M. Herben, *Effect of the Internal Reflection on the Radiation Properties and Input Impedance of Integrated Lens Antennas: Comparisons Between Theory and Measurements*, IEEE Trans. on Microwave Theory and Techniques, Vol. 49, No. 6, June 2001, pp. 1118-1125.

[7] R.A. Wyss, A. Neto, W.R. McGrath, B. Bumble, and H. LeDuc, *Submillimeter-wave spectral response of twin-slot antennas coupled to hot electron bolometers*, Proceedings of 11th Int. Symp. on Space THz Tech., Ann Arbor, MI, May 1-3, 2000.

[8] A. Neto, P.J.I. De Maagt, S. Maci, *Optimized Basis Functions for Slot Antennas Excited by Coplanar Waveguides*, Submitted to IEEE Trans. on Antennas and Propagation (April 5th, 2001, ID AP 0104-0156).

[9] P. Focardi, A. Neto, W. R. McGrath, *Coplanar Waveguide Based, Terahertz Hot Electron Bolometer Mixers: Improved Embedding Circuit Description*, accepted for publication on IEEE Trans. on Microwave Theory and Techniques, N. 0864, Dec. 2001.

[10] Joo-Hiuk Son, Hsi-Huai Wang, John F. Whitaker, Gerard A. Mourou, *Picosecond Pulse Propagation on Coplanar Striplines Fabricated on Lossy Semiconductor Substrates: Modeling and Experiments*, IEEE Trans. on Microwave Theory and Techniques, Vol. 41, No. 9, Page(s) 1574-1580, September 1993.

[11] D.R. Jackson, F. Mesa, M.J. Freire, D.P. Nyquist, C. Di Nallo, *An Excitation Theory for Bound Modes and Residual-Wave Currents on Stripline Structures*, Radio Science, Volume 35, Number 2, Page(s) 495-510, March-April 2000.

[12] A. Neto, S. Maci, *Green's Function of an Infinite Slot Printed Between Two Homogeneous Dielectric. Part I: Magnetic Currents*, Accepted for publication on IEEE Trans. on Antennas and Propagation, ID AP 0107-0350.

[13] K.C. Gupta, *Microstrip Lines and Slotlines*, Ramesh Garg, I.J. Bahl, Artech House 1979.

[14] N. K. Das, *A New Theory of the Characteristic Impedance of General Printed Transmission Lines Applicable When Power Leakage Exists*, IEEE Transactions on Microwave Theory and Techniques, Vol. 48, No. 7, Page(s) 1108-1117, July 2000.

[15] A. Neto, S. Maci, *Input Impedance of an Infinite Slot Printed Between Two Homogeneous Dielectric*, JPL Internal Report, D/21322.

[16] A. Neto, P.H. Siegel, *Equivalent Network Characterization for Series Fed Microstrip Lines on Thin Slabs*, Submitted to IEEE Trans. on Microwave Theory and Techniques (October, 2001, ID 0914).

[17] D. Pasqualini, F. Capolino, A. Toccafondi, S. Maci, *An Improved Evaluation of Radiation Pattern for Dielectric Lens Antennas*, IEEE Antennas and Propagation Symposium, Boston, July 2001.